Detection of short single-strand DNA homopolymers with ultrathin Si_3N_4 nanopores

Jian Ma,[1] Yinghua Qiu,[1] Zhishan Yuan,[1] Yin Zhang,[1] Jingjie Sha,[1] Lei Liu,[1] Litao Sun,[2] Zhonghua Ni,[1,*] Hong Yi, Deyu Li,[3] and Yunfei Chen[1,†]

[1]*Jiangsu Key Laboratory for Design and Manufacture of Micro-Nano Biomedical Instruments, School of Mechanical Engineering, Southeast University, Nanjing 211189, China*

[2]*China Education Council Key Laboratory of MEMS, Southeast University, Nanjing 210096, China*

[3]*Department of Mechanical Engineering, Vanderbilt University, Nashville, Tennessee 37235-1592, USA*

(Received 7 May 2014; published 24 August 2015)

A series of nanopores with diameters ranging from 2.5 to 63 nm are fabricated on a reduced Si_3N_4 membrane by focused ion beam and high energy electron beam. Through measuring the blocked ionic currents for DNA strands threading linearly through those solid-state nanopores, it is found that the blockade ionic current is proportional to the square of the hydrodynamic diameter of the DNA strand. With the nanopore diameter reduced to be comparable with that of DNA strands, the hydrodynamic diameter of the DNA becomes smaller, which is attributed to the size confinement effects. The duration time for the linear DNA translocation events increases monotonically with the nanopore length. By comparing the spatial configurations of DNA strands through nanopores with different diameters, it is found that the nanopore with large diameter has enough space to allow the DNA strand to translocate through with complex conformation. With the decrease of the nanopore diameter, the folded part of the DNA is prone to be straightened by the nanopore, which leads to the increase in the occurrence frequency of the linear DNA translocation events. Reducing the diameter of the nanopore to 2.5 nm allows the detection and discrimination of three nucleotide "G" and three nucleotide "T" homopolymer DNA strands based on differences in their physical dimensions.

DOI: 10.1103/PhysRevE.92.022719 PACS number(s): 87.15.−v, 47.61.Fg

I. INTRODUCTION

Nanopores are promising as single-molecule sensors for the detection and analysis of DNA strands [1–5]. A nanopore sensor measures the modulation of ionic current caused by the physical blockage of a DNA strand in the nanopore. The amplitude and duration of the ionic current modulation depend on the interactions between the DNA molecule and the nanopore. DNA strands are composed of four bases, namely, G, A, T, and C, which have different sizes and surface properties. It is projected that the four bases could lead to different ionic current modulation modes with different amplitudes or durations, based on which a DNA strand could be sequenced as it is threaded through a nanopore. Even though the pioneering research of nanopore sensing is based on protein nanopores, solid-state nanopores, which offer more flexibility in nanopore size and experimental conditions, are later developed and widely studied. Li *et al.* first fabricated a ∼1.8 nm diameter nanopore using ion beam sculpting and demonstrated sensing of double-stranded DNA (dsDNA) molecules [6,7]. Later, Li *et al.* further reported observation of the folding behavior of dsDNA molecules when they translocate a 10 nm diameter solid-state nanopore [7]. Their results indicated that the ionic current blockade for a folded DNA strand was more significant than that for an unfold DNA strand and its duration was shorter than the unfolded one.

While smaller nanopores usually correspond to larger ionic current blockade and hence extend the lower detection limit, it is also important to scale down the thickness of the membrane on which the nanopore is fabricated because the nanopore thickness determines the length of the DNA segment inside the nanopore. For DNA sequencing, the nanopore thickness must be small enough to avoid the averaging effects on signals from many DNA bases. In 2010, Wanunu reported that when the membrane thickness was reduced from 60 to 6 nm, both the open pore current and the ionic current blockade are enhanced; however, the translocation time for a 3 kb dsDNA chain was only marginally affected [8]. Through reducing the membrane thickness and the nanopore diameter, small nucleic acids with as few as ten base pairs can be detected and discriminated based on differences in their physical dimensions. The ideal thickness of a nanopore should be comparable to the distance between two neighboring DNA bases (∼0.34 nm), in which case the ionic current blockade is caused by a single DNA base only. This provides the feasibility of identifying individual DNA bases passing through the nanopore from their signature ionic blockade. The challenge for such thin membranes is their mechanical strength. The membrane becomes extremely fragile as the membrane thickness reduces to just a few nanometers. Recently, two-dimensional graphene membranes of strong in-plane C-C bonds are adopted for fabrication of thin nanopores with diameter below 5 nm [9–14].

While solid-state nanopores are more robust with tunable sizes, they also pose challenges including signal analysis. Naturally occurring nanopores such as α-hemolysin [15–17] and mycobacterium smegmatis porin A [18–20] have fixed geometrical size so the ionic current blockade from identical molecules carries their unique signature. However, for solid-state nanopores, the challenging nanofabrication process renders inevitable size variation, leading to very different ionic current blockades even when the same DNA strands pass through two different nanopores. Therefore, it is important to explore the effects of various parameters, such as the nanopore dimension, molecule size, and electrolyte concentration, on

*Corresponding author: nzh2003@seu.edu.cn
†Corresponding author: yunfeichen@seu.edu.cn

the ionic current blockade when a molecule translocates the nanopore [8,21–23]. In general, the ionic current through a nanopore can be estimated through considering the size and shape of the nanopore together with the properties of the electrolyte used. However, for small enough nanopores, electric double layers overlap inside the nanopore, which could induce significant concentration changes for both counterions and coions. As a result, the ionic current may depend not only on the nanopore size but also on the surface charge densities of the nanopore and the molecules. Wanunu *et al.* introduced a modified model to take into account the change of the ion concentration, in which a fitting parameter was introduced, which could pose some challenges in applying this model for different cases [8].

In this paper, a series of nanopores with different lengths and diameters are fabricated to investigate various factors that affect the ionic current through nanopores. It is found that the geometrical model can still approximately predict the ionic current blockade, which helps to establish a relation between ionic current blockade and the duration to distinguish the data produced from different nanopores. Based on these studies, we further extract various spatial configurations of DNA strands when they translocate nanopores with different diameters. It is found that the nanopore with large diameter has enough space to allow for DNA strands passing through with complex conformations [24]. However, as the nanopore diameter decreases, the folded part of the DNA is prone to be straightened by the steric force. When the diameter of the nanopore is reduced to 7 nm, the λ-DNA will gather in the nanopore entrance and then crowd around the mouth of the nanopore, which further reduces the nanopore diameter. The interactions between the nanopore inner surface and DNA strands and the heavy traffic of DNA across the nanopore will significantly slow down the DNA translocation speed. It is demonstrated that the nanopore of 2.5 nm in diameter and 8 nm long can distinguish single-strand three nucleotide (nt) "G" and three nt "T" DNA homopolymers based on the difference in their physical dimensions.

II. FABRICATION OF NANOPORES AND EXPERIMENTAL SETUP

A schematic nanopore fabrication process is given in Fig. 1. A 100-nm-thick silicon nitride membrane was first deposited by low pressure chemical vapor deposition on a silicon wafer. A window of $100 \times 100\,\mu m^2$ was etched from the back side of the silicon wafer by tetramethylammonium hydroxide wet etching until the silicon nitride is exposed. With a focused ion beam [Ga^+ ion beam in the FEI Helios 600i focused ion beam (FIB) system operated at 30 kV], a circular area was then milled on the front side of the membrane to reduce the film thickness. Note that the "milling" process is monitored *in situ* with the scanning electron microscope in the FEI Helios 600i system.

The depth of the thinning area can be tuned by setting the milling time and the ion beam intensity. Figure 1(c) plots the milling depth as a function of the milling time for the FIB operated at two ion beam currents of 1.1 and 7.1 pA, respectively, indicating good linear relationships between the milling depth and the milling time for both cases. While a higher ion current removes the Si_3N_4 more efficiently, it is easier to control the milling depth with a low beam current setting. As such, we chose to conduct the milling process with the low ion beam current (1.1 pA) to reduce the film thickness. Based on the relation between the milling time and the milling depth, the remaining film thickness can be approximately

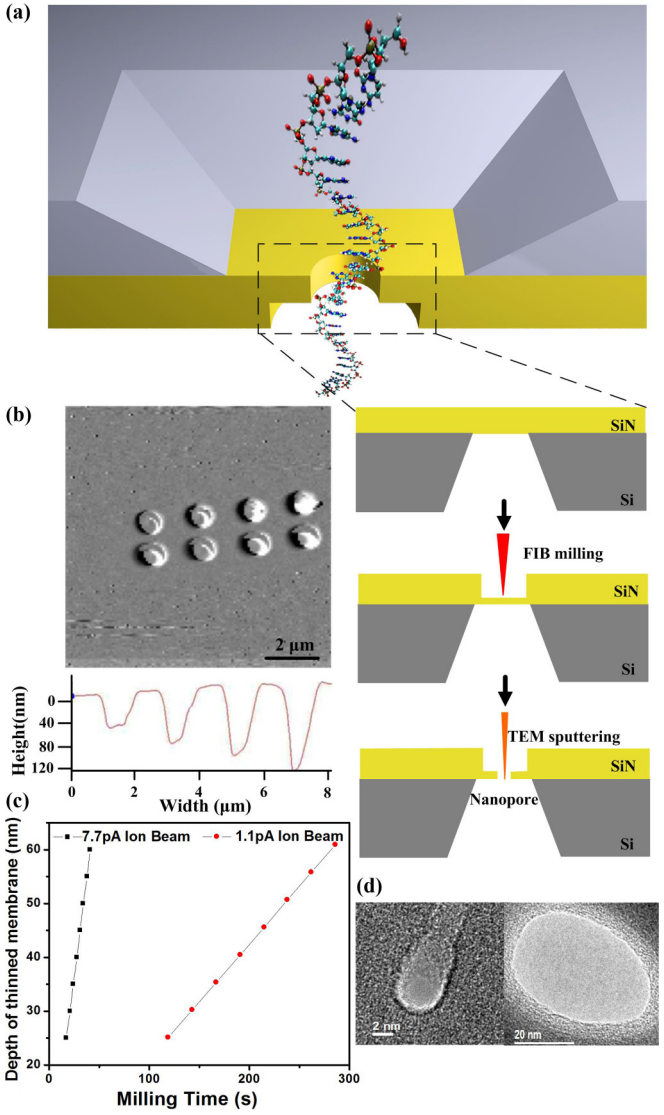

FIG. 1. (Color online) Ultrathin Si_3N_4 nanopore fabrication and characterization. (a) Scheme of a nanopore sensor showing a DNA molecule translocating through the pore. The sensor consists of a $2.5 \times 2.5\,mm^2$ silicon chip that contains a freestanding Si_3N_4 membrane ($100 \times 100\,\mu m^2$). After the process of FIB milling a circular area on the thick Si_3N_4 membrane, a nanopore is sputtered using a TEM on the thinned area. (b) AFM topography image of a 4×2 circle array following FIB milling process, as well as a line profile that shows the depth of the trenches. (c) The etched depth is a linear function of the etched time and the etched rate is totally up to the size of the ion beam. The red point is for the focused ion beam operated at 1.1 pA and the blue point is operated at 7.7 pA. (d) Transmission electron micrograph of two typical nanopores: the first one has a diameter at 2 nm fabricated by TEM; the second one is fabricated by FIB. It looks like an oval; the longest length is about 45 nm and the smallest length is about 35 nm.

controlled, which was also measured with an atomic force microscope, as shown in Fig. 1(b). Characterization showed that Si_3N_4 membranes less than 10 nm thick could be reliably achieved.

Another important parameter that directly determines the mechanical properties of the membrane is the size of the thinned region. Figure 1(b) presents an atomic force microscopy (AFM) topography image of a 4×2 circle array following the FIB milling process, as well as a line profile that shows the depth of the holes. It is found that the membrane became more fragile and could be broken easily with the increase of hole depth. Another factor that is important for the membrane strength is the diameter of the hole, which is set to range from 500 to 1000 nm. Once the Si_3N_4 membrane is reduced to a specified thickness, a transmission electron microscope (TEM, FEI Titan80-300) was used to fabricate the nanopore in the center of the thinned region. The size of the nanopore could be tuned by adjusting the electron beam intensity [6,25].

A series of nanopores with diameters ranging from 2 to 20 nm have been fabricated using the above described process. The minimum length of the nanopore is below 10 nm through thinning the Si_3N_4 membrane with the focused ion beam. For nanopores with diameters larger than 20 nm, we can fabricate them with the focused ion beam directly without involving the TEM. Using both FIB and TEM, we successfully prepared nanopores with a wide range of dimensions (diameters ranging from 2.5 to 63 nm and lengths ranging from 8 to 100 nm). Figure 1(d) shows the TEM micrographs of two nanopores of 2.5 and 40 nm in diameter, respectively.

In order to measure the resistive pulse response during DNA translocation through a nanopore, the Si_3N_4 membrane was cleaned with piranha solution before being installed between two fluidic chambers. The cleaning process helps to remove contaminations from the fabrication process and reduce the $1/f$ noise [21]. Silicone elastomer rubber was used to seal the Si_3N_4 membrane between the two chambers and the two chambers are clamped by a mini bench vice. Ag/AgCl electrodes are immersed in the two chambers filled with buffered NaCl electrolytic solution. A patch clamp amplifier (EPC 10 USB, HEKA Instruments, Germany) is connected to the two Ag/AgCl electrodes to measure the changes in ionic current with a picoampere sensitivity. The whole setup is enclosed in a double Faraday cage to reduce electrical noise from the environment [26,27]. The EPC 10 USB patch clamp amplifier supports a signal bandwidth as high as 200 kHz. Using a higher sampling rate is beneficial to collect more data, but associated with larger noise. All of 48 kb λ-DNA samples were detected at 20 kHz sampling rate and low-pass filtered at 10 and 2.9 kHz with a two-pole Bessel filter. When detecting the short single DNA homopolymers, we increased the sampling rate to 50 kHz. The frequency of the second filter is reduced to 1 kHz in order to minimize the noise.

III. EXPERIMENT RESULT AND DISCUSSION

All measurements are conducted with 1 M NaCl salt solution containing 10 mM Tris and 1 mM ethylenediaminetetraacetic acid at pH 7.0 at room temperature. DNA molecules (purchased from Dalian Takara Biotechnology Co., Ltd) are dispersed into the salt solution at the *cis* side. In selecting the solution used, we considered both NaCl and LiCl following the report by Kowalczyk *et al.* that Li^+ and Na^+ bound DNA stronger than K^+ [28]. The counterion binding to DNA provides a practical method for slowing down the translocation by at least tenfold. We tried 1 M LiCl salt solution but did not observe any translocation events. This could be due to the fact that the Li^+ counterions almost completely neutralized the negative charge of the DNA. As such, we chose NaCl solution in our experiment and under an applied electrical field, the DNA strands were driven through the nanopore.

As shown in Fig. 2(a), continuous current traces with a series of spikes were detected with the patch clamp amplifier. There is a decay in the ionic current at the beginning of each scan trace due to the capacitive effects. To avoid any complications from this decay, when we examined the translocation events, we only considered the events from the ionic currents in the regime with a stable baseline current. Each spike represents an interaction event between the DNA strand with the nanopore because the physical blockage of the nanopore by the DNA strand causes a down peak in the ionic current. The amplitude of the ionic current blockade is defined as the difference between the ionic current through the nanopore in the open state and that in the blocked state, which reads as

$$\Delta I = I_{\text{open}} - I_{\text{blocked}}. \quad (1)$$

According to the amplitude and the duration of a blockade event, it is possible to distinguish whether the DNA passes through the nanopore in folding or unfolding configuration [7,24]. As shown in the bottom inset of Fig. 2(a), there exist six types of signal modes for the blockade events from the translocation of λ-DNA strands through a 63-nm-diameter nanopore. The histogram of the current blockade magnitude is plotted in the upper-right inset of Fig. 2(a).

The simplest mode is for the downward spike with only one flat bottom, which corresponds to the case that the DNA is threaded through the nanopore in a linear fashion. Other modes include those spikes with two blockade levels, which come from translocations of folded DNA strands. The folded section leads to an ionic current blockade that is approximately twice the magnitude of an unfolded DNA strand. The six modes of the current blockade as the λ-DNA molecules translocate the 63-nm-diameter nanopore are described in the bottom inset of Fig. 2(a). The first represents an unfolded DNA and the second stands for a fully folded DNA translocating the nanopore. The third mode implies that the DNA is partially folded at the front and the fourth one comes from that the DNA is partially folded at the tail. The fifth mode mostly results from a DNA strand that has a knot in the middle, while the last one originates from a DNA that is partially folded at both the front and the tail.

These rich possibilities for DNA strands to take various configurations across a nanopore are attributed to the large size of the nanopore, which imposes little steric constriction on the DNA strand. For smaller nanopores, the interaction between the nanopore and DNA strands becomes stronger, which leads to a higher energy barrier for DNA translocation across the nanopore. The enhanced energy barrier is beneficial for straightening the DNA strand. As a result, fewer ionic current blockade modes are observed. For example, no event with the DNA knotted in the middle and partially folded at both the front and tail was observed for the other

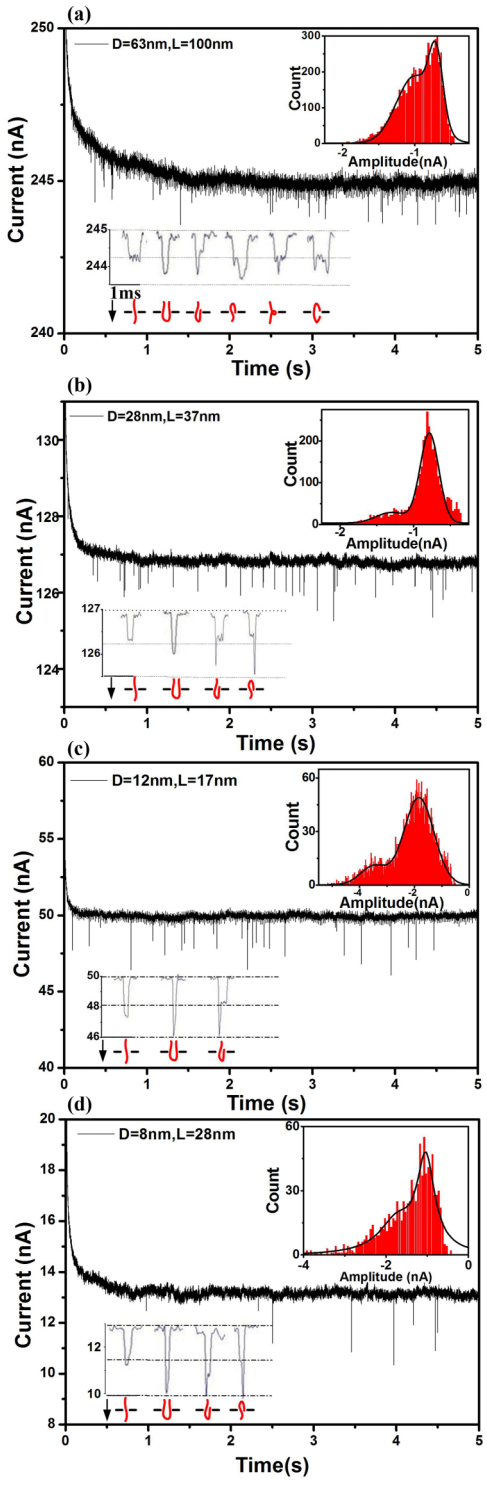

FIG. 2. (Color online) DNA translocation through different size nanopores. Data are taken in 1 M NaCl solution at 1 V bias voltage and filtered at 10 kHz for display. (a). The spikelike current trace in a 63-nm-diameter, 100-nm-long nanopore. The upper inset shows the amplitude histograms of all events. The lower inset shows examples of amplified signals that are observed, accompanied with the interpretation of the DNA spatial configuration while they translocate the nanopore. (b) The data collected from a 28-nm-diameter, 37-nm-long nanopore. (c) The data correspond to a 12-nm-diameter, 17-nm-long nanopore. (d) The data for an 8-nm-diameter, 28-nm-long nanopore.

three pores with diameters of 28, 12, and 8 nm, as shown in Figs. 2(b)–2(d). It is found that when λ-DNA strands translocate a 28-nm-diameter pore, only the first four modes of blockades observed for the 63 nm nanopore can be detected. Reducing the nanopore diameter to 12 nm further limits the allowable spatial configurations to three types.

The partially folded configurations occurred for both the 28 and the 12 nm nanopores; however, for the 28 nm pore, the folded segment could be at either the front or the tail, while for the 12 nm nanopore, only one partially folded configuration at the front was observed. This is most probably due to the fact that the smaller nanopore provides larger drag force to straighten the coiled DNA. Interestingly, however, for the 8-nm-diameter pore, signals for partially folded DNA at both the front and tail were detected again, indicating that the allowable DNA configurations are not solely determined by the nanopore diameter. In addition to the pore diameter, the thickness of the pores can also play an important role. The thickness of the 12-nm-diameter pore is ∼17 nm, which is smaller than the ∼28 nm of the 8-nm-diameter nanopore. Since the dominant voltage drop is across the nanopore, a thicker nanopore corresponds to a lower electric field intensity inside the nanopore, as long as the same bias voltage is applied to the two chambers. As such, when DNA strands translocate the 12-nm-diameter pore, they experience a stronger electrophoretic force than that as they pass through the 8-nm-diameter pore. As a result, any folding at the tail of the DNA strand will be straightened for the case of the 12-nm-diameter pore.

A scatter plot of the blocked current ΔI versus the duration for different size nanopores is given in Fig. 3. As shown in Fig. 3(a), significant overlap exists between data from different pores, which makes it difficult to do signal analysis. Since the signal is caused by the physical blockage of the nanopore by the DNA strands, the magnitude and duration of the ionic current blockade should depend on the relative size of the nanopore and the DNA molecule. It is worth noting that for naturally occurring protein nanopores such as α-hemolysin, the pore size is the same as long as the same type pore is used and there is no need to consider the effects of different pore size on detected signals. However, for fabricated solid-state nanopores, even the same DNA strands may induce different signal modes when they pass through different nanopores. As such, it is important to determine the correlations between the ionic current blockade and the DNA molecule to extract more information from the measurement.

The ionic current blockade may provide useful information about the nanopore geometry. As shown in Fig. 3(a), the four nanopores present different ionic current blockade amplitudes even for identical 48 kb λ-DNA strands. Based on a simplified geometrical model, it is possible to establish a relation between the ionic current blockade and the nanopore size. The ionic current modulation can be calculated as [8,21]

$$\Delta I = I_{\text{open}} - I_{\text{blocked}} = \frac{V e(\mu_{\text{Na}^+} + \mu_{\text{Cl}^-})\pi}{4h} \times \left[n_{\text{NaCl}} d_{\text{pore}}^2 - n^*_{\text{NaCl}}\left(d_{\text{pore}}^2 - d_{\text{DNA}}^2\right)\right], \quad (2)$$

where V is the voltage drop across the nanopore; μ_{Na^+} and μ_{Cl^-} are the mobility of sodium and chloride ions, respectively; h is the effective thickness of the nanopore; d_{pore} is the diameter

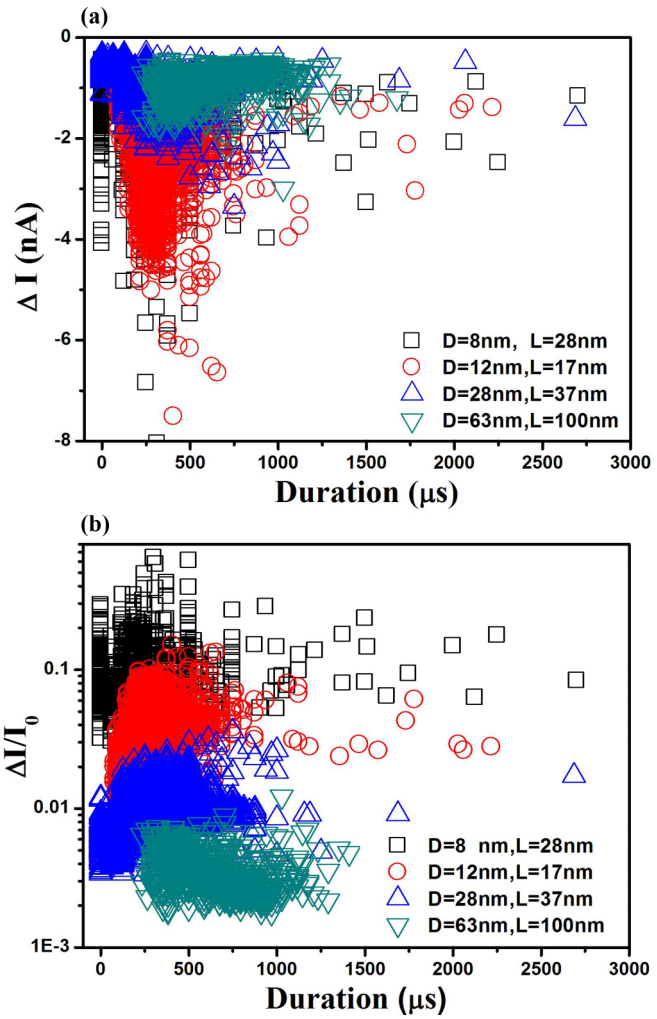

FIG. 3. (Color online) (a) Scatter diagram of the amplitude of the ionic current blockade versus translocation time for DNA translocation through four nanopores. (b) Scatter plot of the relative ionic current change versus the duration.

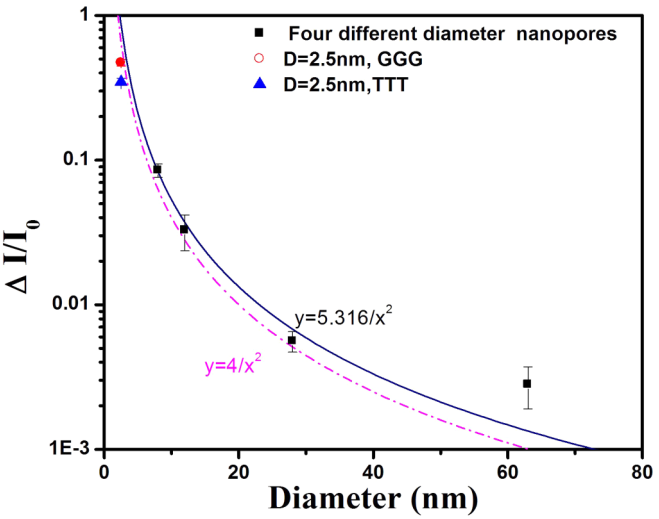

FIG. 4. (Color online) The ratio of the ionic current blockade to the baseline current for DNA translocating nanopores in a linear configuration versus the nanopore diameter. The best fit curve from our fitting procedure is the function of $5.316/x^2$ (black curve). The purple dash-dotted curve corresponds to the theoretical model with the diameter of dsDNA molecules estimated as 2 nm.

of the nanopore; d_{DNA} is the hydrodynamic diameter of the DNA and e is the elementary charge; and n_{NaCl} and n^*_{NaCl} are the concentration of sodium and chloride ions inside the nanopore before and after the DNA molecule enter the pore. When a DNA strand occludes the nanopore, it will exclude part of the anions due to electrostatic repulsion and decrease the effective concentration of anions. On the other hand, the DNA molecule also brings more cations into the nanopore, which increases the cation concentration in the nanopore. For high salt solution, it is common to neglect the difference between n_{NaCl} and n^*_{NaCl}, and the ionic current blockade ΔI can be approximated as [26,29,30]

$$\Delta I \approx I_0 \left(\frac{d_{\mathrm{DNA}}}{d_{\mathrm{pore}}} \right)^2 . \tag{3}$$

This formula indicates that the ionic current blockade is proportional to the baseline current and inversely proportional to the square of the nanopore diameter. It can be seen from Eq. (3) that the ratio of the ionic current blockade to the baseline is a function of the diameter ratio of the DNA strand to the nanopore only. In Fig. 3(b), we plot the relative ionic current modulation versus the duration, in which case the data obtained from different nanopores are distributed in different regions. This indicates that the relative ionic current modulation is more sensitive to the molecular size in nanopore-based sensing.

As shown in Fig. 2, λ-DNA strands translocate the four types of nanopores in different configurations, which results in a wide distribution of the magnitude and duration in the detected ionic current blockade. Another reason for the wide distributed data in Fig. 3(b) is the complex interactions between the DNA strand and the nanopore. For example, the longest duration observed is ∼3000 μs, which must come from a strong interaction between the dsDNA molecule and the nanopore surface during the translocation process [12,31–33].

Since the ionic current blockade from the folded DNA conformation cannot provide any useful information to identify single nucleotides, we focus our analysis on the events corresponding to DNA translocation through the nanopores in a linear configuration. The duration and current blockade amplitude for DNA translocation in the linear configuration can be obtained through fitting the current histogram with the Gaussian distribution function.

Figure 4 depicts the ratio of the ionic current blockade to the baseline current for DNA translocation through nanopores in a linear configuration versus the nanopore diameter. The four square data points correspond to the relative ionic current blockade for nanopores of 8, 12, 28, and 63 nm diameter, respectively. A least square method is used to fit the four points with a function of A/x^2, which yields a best fitting curve as $5.316/x^2$. It is worth noting that we can also estimate the parameter A from Eq. (3), according to which A should be equal to the square of the DNA diameter. In our experiments, double-strand λ-DNAs are used, whose diameter can be estimated as ∼2 nm [34]. Therefore, the theoretical value of A is smaller

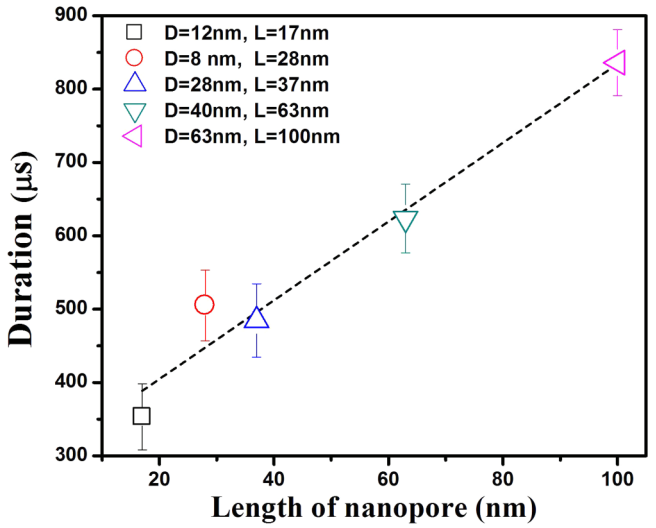

FIG. 5. (Color online) The mean duration of unfolded DNA translocation events for DNA translocation through five nanopores with different diameters and lengths measured in 1 M NaCl solution at 1000 mV.

than the best fitting value of 5.316. The measured ionic current modulation for nanopores with >8 nm diameter is larger than the prediction from the theoretical model.

In addition to the relatively large nanopores with >8 nm diameter, we have also fabricated nanopores with ∼2.5 nm diameter and used them to detect single-strand DNA homopolymers with three nt "G" and three nt "T." The relative current blockades for these two strands are also plotted in Fig. 4. Interestingly, the two data points are below both the fitted curve and the theoretical curve based on the simple geometrical model, which prompts us to consider the effects of nanopore size at different scales on the ionic current blockade. Our data indicate that the hydrodynamic diameter of DNA strands is underestimated when the nanopore diameter is far larger than the diameter of a DNA strand. However, when the nanopore size is reduced to be comparable with the DNA diameter, the hydrodynamic diameter of DNA strands will be reduced accordingly due to the size confinement effect and can be approximated with the DNA physical diameter.

Figure 5 presents the mean translocation time for unfolded λ-DNAs passing through five nanopores of different diameters and lengths under the same applied electrical bias and salt concentration. The speed of the DNA crossing a nanopore directly depends on the driving force induced by the external electrical field. Under the same applied voltage, the electric field intensity in the nanopore reduces with the increase of the nanopore length, leading to reduced driving force. The monotonic increase of the translocation time with the nanopore length is a direct result of the reduced electric field strength in longer pores [35,36]. Our data show that overall the translocation time increases linearly with the nanopore length, while the data point for the 28-nm-long nanopore deviates significantly from the line. The diameter of the 28-nm-long nanopore is 8 nm, which is the smallest among all the nanopores shown in Fig. 5. To explore whether this small diameter is related to the longer translocation time, we further reduce the pore diameters and observe its interaction with the rather long 48 kb λ-DNA molecules.

As the diameter is reduced to 7 nm, it was found that the 48 kb λ-DNA can still translocate the nanopore. However, with the elapse of time, the baseline ionic current will reduce from 32 to 16 nA step by step, as shown in Fig. 6(d). We speculate that this is due to accumulation of the 48 kb λ-DNA at the mouth of the nanopore with some section of each molecule dangling inside the pore, which effectively reduces the nanopore diameter. This process is illustrated in Figs. 6(a) and 6(b). In fact, the trace in Fig. 6(d) suggests that the ionic current reduces by ∼2 nA with each additional DNA segment entering the nanopore. During this accumulation process, the translocation events can still be observed, which implies that the λ-DNA is still allowed to pass through the pore with reduced size. However, when the baseline current dropped to 16 nA, the translocation events almost stopped. However, if we added 30 nt "G" DNA homopolymers at the *cis* side, we found that these smaller molecules could still translocate the modified pore, as evidenced by the spikes riding on the 16 nA baseline.

In order to distinguish which DNA strands cause the translocation events, the blockade signals are further analyzed. The ratio of the ionic current blockade to the baseline current is about 0.03, smaller than the 0.059 for the λ-DNA translocation events. As such, these translocation events should be from the single-strand 30 nt "G" DNA homopolymers. In addition, the interactions between the crowded λ-DNA and the 30 nt "G" DNA homopolymers significantly slowed down the translocation speed. Figure 6(e) plots the relative ionic current blockade amplitude versus the duration. Before the nanopore is modified by the 48 kb λ-DNA, the mean duration for the translocation of the 48 kb λ-DNA is about 520 μs. After the nanopore was crowded by the 48 kb λ-DNA, the mean translocation time for the 30 nt "G" is about 897 μs, which is even longer than that for the 48 kb λ-DNA. The inset in Fig. 6(e) shows the *I-V* curve of the 7 nm nanopore before and after the 48 kb DNA crowded the nanopore. It can be seen that without the 48 kb λ-DNA accumulated at the nanopore, the *I-V* curve is linear; however, after the nanopore is crowded with the 48 kb λ-DNA, the *I-V* curve shows a rectified feature, which is due to the presence of the negatively charged DNA molecules inside the pore. It is worth noting that this measurement was conducted with 1 M NaCl solution, and the rectification effect could be much more pronounced with lower salt concentration.

We also prepared a nanopore of 2.5 nm diameter and used it to study the DNA translocation phenomena. At this size, translocation of the 48 kb λ-DNA strands can be rarely seen because of the strong steric force from the tiny pore and the complex, entangled configuration of the long DNA chain. We then replaced the 48 kb λ-DNA strands with shorter single-strand DNA homopolymers. Three kinds of short single-strand DNA homopolymers, including 30 nt "G," 3 nt "G," and 3 nt "T" are placed into the *cis* side separately for the translocation experiments. Before adding each kind of DNA homopolymers, both the chambers and the nanopore are thoroughly cleaned to ensure that there is no residual from the previously used DNA homopolymers. Figure 7(a) displays the continuous current trace for the homopolymers of 30 nt

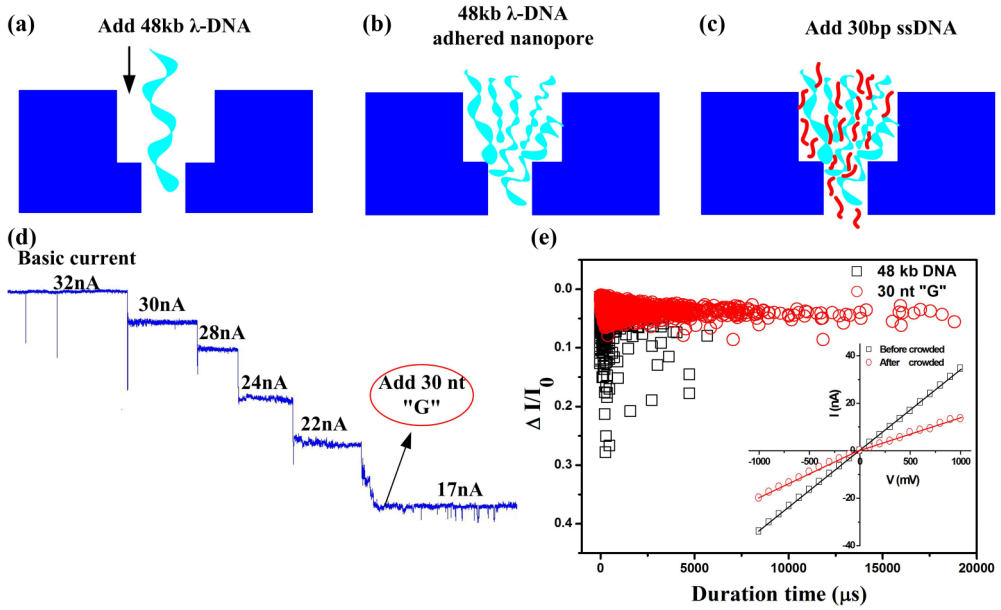

FIG. 6. (Color online) (a) At the beginning, 48 kb λ-DNA can translocate through a 7-nm-diameter nanopore. (b) With the elapse of the time, 48 kb λ-DNA will crowd the mouth of the nanopore until they cannot pass anymore. (c) After the base ionic current is stabilized again, 30 nt "G" single-strand DNA homopolymers are added in the *cis* side chamber. The smaller homopolymers can still pass through the crowded nanopore. (d) Continuous current trace shows the baseline ionic currents decreased step by step due to the λ-DNA strands accumulated in the nanopore, which is reduced from 32 to 16 nA step by step. (e) Scatter plot of the relative blockade current versus the duration for 48 kb λ-DNA before the nanopore is crowded and for 30 nt "G" single-strand DNA homopolymers after the nanopore is crowded by the λ-DNA. The inset shows the *I-V* curve before and after the 48 kb λ-DNA crowded the nanopore.

"G," 3 nt "G," and 3 nt "T" translocating the 2.5-nm-diameter nanopore in 1 M NaCl solution under a 1000 mV applied bias. Figure 7(b) demonstrates the amplified signals from the three kinds of DNA homopolymers. From these amplified signals, a common feature exists for the continuous current traces of all three types of homopolymers, which have two downward spike levels. It looks like the DNA homopolymers accumulate around the nanopore mouth first and then they manage to squeeze through the nanopore. Figure 7(c) gives a schematic illustration of such translocation process.

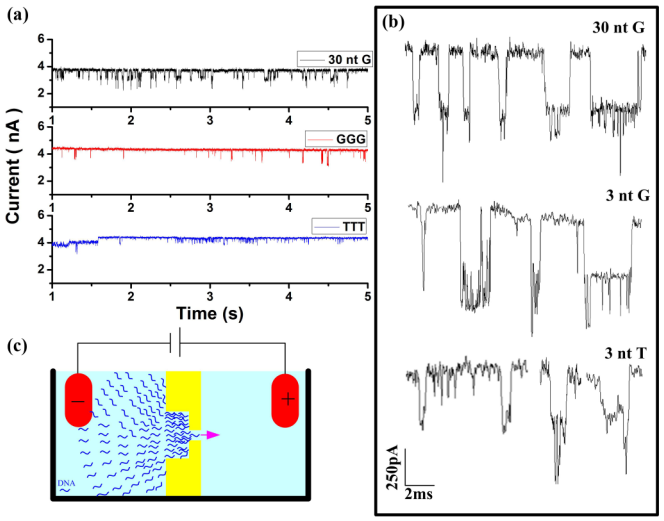

FIG. 7. (Color online) (a) Continuous current traces for 30 nt "G" (black), 3 nt "G" (red), and 3 nt "T" (blue) translocating through a 2.5-nm-diameter nanopore, respectively, measured at 1000 mV in 1 M NaCl solution. (b) Amplified blockade signals corresponding to the three kinds of DNA homopolymers across the nanopore in (a), respectively. (c) Schematic illustrations of the short DNA strands across the 2.5-nm-diameter nanopore.

Previous studies have shown that the capture mechanism of a dsDNA involves two main steps. First, as a DNA coil approaches the pore from bulk solution to a distance larger than the coil size, its motion transitions from purely diffusive to biased drift, driven by the electric field outside the pore. In the second step, once the DNA coil is within approximately one coil size from the pore, one end of the DNA threads into the pore, a process that involves crossing a free-energy barrier [29,37,38]. In our nanopore mouth, there is a 500-nm-diameter, 92-nm-deep cylindrical pore milled by the focused Ga^+ ion beam. During the DNA homopolymers translocation through the nanopore, the DNA homopolymers first accumulate inside this large cylindrical pore, which results in many DNA homopolymers crowding around the mouth of the nanopore. This traffic congestion markedly slows down the DNA translocation speed. Figure 7(c) is a sketch of the process of DNA homopolymers accumulating inside the cylindrical pore and then squeezing through the nanopore. With the increase of the local DNA homopolymer concentrations in the nanopore mouth, it is also possible to form G quadruplexes, which may also prolong the translocation time.

Figure 8(a) plots the ionic current blockade amplitude versus the duration for 30 and 3 nt G single-strand DNA homopolymers translocating the 2.5-nm-diameter nanopore. The thickness of the Si_3N_4 film on which the nanopore resides is 8 nm. As shown in Fig. 8(b), there are two levels of ionic

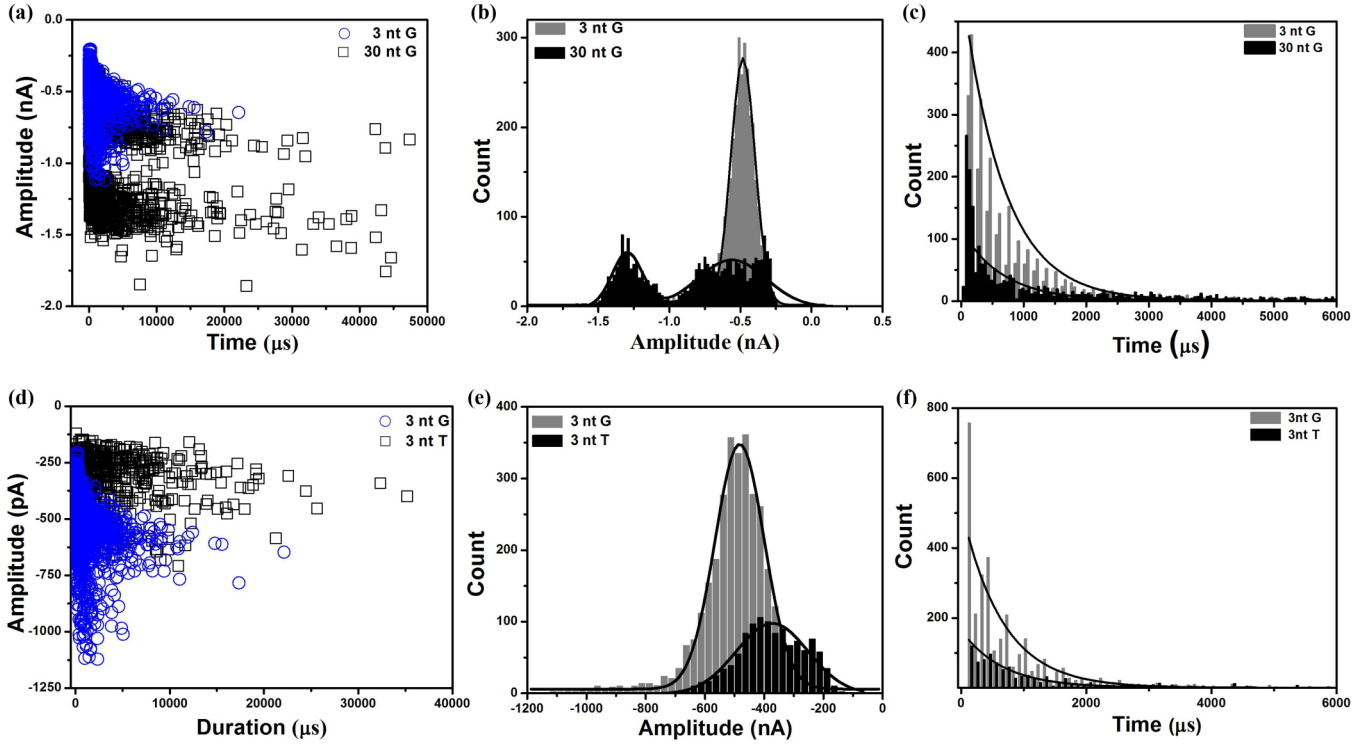

FIG. 8. (Color online) Differentiation of short single-strand DNA homopolymers in a 2.5-nm-diameter and 8-nm-long nanopore. (a) Scatter plot of the current blockade versus the duration time of 30 nt "G" and 3 nt "G" homopolymers. (b) The frequency histogram of two kinds of homopolymer blockade amplitude with the Gaussian fit. (c) Histograms of 30 nt "G" and 3 nt "G" translocation time of events. (d) Scatter plot of the blockade current versus the translocation time of three nt "G" and three nt "T" homopolymers. (e) The amplitude histogram of the two kinds of homopolymer translocation events with the Gaussian fit. The amplitude of the blocked current of "G" is located in 0.51 nA, while "T" is located in 0.375 nA. (f) Histograms of three nt "G" and three nt "T" translocation time of events.

current blockades for the 30 nt "G" DNA homopolymer. The first type is with an ionic current blockade of ∼0.51 nA, while the second one is with a blockade of ∼1.3 nA. This large ionic current blockade might be caused by the basket fold G quadruplexes structure [39–42]. The ratio of the second amplitude to the first amplitude is about 2.5. This ratio is close to the cross-sectional area ratio between G quadruplexes and a single G homopolymer.

Figure 8(d) plots the ionic current blockade amplitude versus the translocation time for the homopolyers three nt "G" and three nt "T" translocating the 2.5-nm-diameter nanopore in 1 M NaCl solution under 1000 mV applied bias. The volume of G is about 359 $Å^3$ and its cross-sectional area is about 56 $Å^2$, while the volume of T is about 339 $Å^3$ with a cross-sectional area of about 37 $Å^2$ [43]. In order to quantify the difference between the two molecules, we compare these events by analyzing the scatter plots of the modulation in ionic current versus the duration. Figure 8(e) shows the histogram of the current blockade plotted in Fig. 8(d). The amplitudes of the current blockades for three nt "G" and three nt "T" are $\Delta I_G = 0.5$ nA and $\Delta I_T = 0.375$ nA, respectively, which suggests that the 2.5-nm-diameter nanopore could be able to distinguish the three nt "G" and three nt "T." To observe the effects of the nucleotide size, we compare the ratios of the ionic current blockade and the cross-sectional area between three nt "G" and three nt "T." The ratio of the ionic current blockade for three nt "G" and three nt "T," $\Delta I_G/\Delta I_T = 1.33$, is smaller than the ratio of their cross-sectional area, $A_G/A_T = 1.51$. This implies that the ionic current blockade does not depend solely on the molecule size. Therefore, when the nanopore size is comparable to the molecule size, the change of the ion density inside the nanopore induced by the molecules should be taken into accounted, as discussed in Refs. [8,21].

In the case of DNA translocation through nanopores without interactions between the DNA molecules, the translocation events should follow a Poisson process with an exponential distribution [29]. Figures 8(c) and 8(f) show the histograms of 30 nt "G," 3nt "G," and 3 nt "T" homopolymers translocation time. The distribution can be approximated by an exponential function, which indicates that any interactions between the molecules would cause deviations from Poisson distribution.

IV. CONCLUSION

In this paper, a series of nanopores with different lengths and diameters are fabricated with FIB and TEM. It is demonstrated that the Si_3N_4 membrane can still provide mechanical strength robust enough to support a nanopore even when its thickness is reduced below 10 nm. Those nanopores are used to observe the DNA spatial conformations in a confined space. It is founded that the coiled DNA molecules can be straightened more fully in the smaller and thinner nanopore by the external electrical field. The thinned nanopore increases the signal amplitudes of biomolecules but speeds up the DNA translocation through the nanopore. However,

once the nanopore diameter is reduced to be comparable with the biomolecule size, it may enhance the interaction strength between the molecules and the wall of the nanopores, which causes the decrease of the DNA translocation speed. With the continued decrease of the nanopore diameter, the hydrodynamics diameter of a DNA strand will also be reduced due to the size confinement effects. Our work demonstrated that the relative blockade ionic current can be roughly predicted with the simply geometrical model that accounts for the nanopore size and the biomolecule size. With the use of the geometrical model, it is possible to distinguish the data points produced from different nanopores. This is important for the application of solid-state nanopores. Our work also demonstrated that single-strand DNA homopolymers three nt "G" and three nt "T" can be distinguished from their blockade ionic current amplitudes with the 2.5-nm-diameter nanopore.

ACKNOWLEDGMENTS

The authors thank the National Basic Research Program of China (Grants No. 2011CB707601 and No. 2011CB707605), Natural Science Foundation of China (Grants No. 51435003, No. 51003015, No. 50925519, and No. 51005048), and the Jiangsu Province Nature Science Foundation (Grant No. BK2009292) for financial support. D.L. appreciates the financial support from the U.S. National Science Foundation (CBET#1067213).

J.M. and Y.Q. contributed equally to this work. J.M., Y.Q., Z.N., and Y.C. designed the experimental work. Y.Z., Z.Y., J.S., and L.L. designed the microchannel and the measurement processes. J.M. and Z.Y. fabricated the microchip and nanopore. Y.Q., Z.N., L.S., H.Y., D.L., and Y.C. analyzed and discussed the measured data. J.M., Y.Q., and Y.C. prepared the manuscript.

[1] K. Healy, B. Schiedt, and A. P. Morrison, Nanomedicine (London, UK) **2**, 875 (2007).
[2] J. J. Nakane, M. Akeson, and A. Marziali, J. Phys.: Condens. Matter **15**, R1365 (2003).
[3] B. M. Venkatesan and R. Bashir, Nat. Nanotechnol. **6**, 615 (2011).
[4] L. Ma and S. L. Cockroft, ChemBioChem **11**, 25 (2010).
[5] S. Howorka, S. Cheley, and H. Bayley, Nat. Biotechnol. **19**, 636 (2001).
[6] J. Li, D. Stein, C. McMullan, D. Branton, M. J. Aziz, and J. A. Golovchenko, Nature (London) **412**, 166 (2001).
[7] J. L. Li, M. Gershow, D. Stein, E. Brandin, and J. A. Golovchenko, Nat. Mater. **2**, 611 (2003).
[8] M. Wanunu, T. Dadosh, V. Ray, J. M. Jin, L. McReynolds, and M. Drndic, Nat. Nanotechnol. **5**, 807 (2010).
[9] G. F. Schneider, S. W. Kowalczyk, V. E. Calado, G. Pandraud, H. W. Zandbergen, L. M. K. Vandersypen, and C. Dekker, Nano Lett. **10**, 3163 (2010).
[10] S. Garaj, W. Hubbard, A. Reina, J. Kong, D. Branton, and J. A. Golovchenko, Nature (London) **467**, 190 (2010).
[11] T. Xu, K. B. Yin, X. Xie, L. B. He, B. J. Wang, and L. T. Sun, Small **8**, 3422 (2012).
[12] G. F. Schneider, Q. Xu, S. Hage, S. Luik, J. N. H. Spoor, S. Malladi, H. Zandbergen, and C. Dekker, Nat. Commun. **4**, 2619 (2013).
[13] Z. S. Siwy and M. Davenport, Nat. Nanotechnol. **5**, 697 (2010).
[14] C. A. Merchant *et al.*, Nano Lett. **10**, 2915 (2010).
[15] D. Stoddart, A. J. Heron, E. Mikhailova, G. Maglia, and H. Bayley, Proc. Natl. Acad. Sci. USA **106**, 7702 (2009).
[16] T. Z. Butler, J. H. Gundlach, and M. A. Troll, Biophys. J. **90**, 190 (2006).
[17] Y. L. Ying, C. Cao, and Y. T. Long, Analyst **139**, 3826 (2014).
[18] I. M. Derrington, T. Z. Butler, M. D. Collins, E. Manrao, M. Pavlenok, M. Niederweis, and J. H. Gundlach, Proc. Natl. Acad. Sci. USA **107**, 16060 (2010).
[19] T. Z. Butler, M. Pavlenok, I. M. Derrington, M. Niederweis, and J. H. Gundlach, Proc. Natl. Acad. Sci. USA **105**, 20647 (2008).
[20] E. A. Manrao, I. M. Derrington, A. H. Laszlo, K. W. Langford, M. K. Hopper, N. Gillgren, M. Pavlenok, M. Niederweis, and J. H. Gundlach, Nat. Biotechnol. **30**, 349 (2012).
[21] R. M. M. Smeets, U. F. Keyser, D. Krapf, M. Y. Wu, N. H. Dekker, and C. Dekker, Nano Lett. **6**, 89 (2006).
[22] A. T. Carlsen, O. K. Zahid, J. Ruzicka, E. W. Taylor, and A. R. Hall, ACS Nano **8**, 4754 (2014).
[23] S. C. Kim, S. K. Kannam, S. Harrer, M. T. Downton, S. Moore, and J. M. Wagner, Phys. Rev. E **89**, 042702 (2014).
[24] P. Chen, J. J. Gu, E. Brandin, Y. R. Kim, Q. Wang, and D. Branton, Nano Lett. **4**, 2293 (2004).
[25] A. J. Storm, J. H. Chen, X. S. Ling, H. W. Zandbergen, and C. Dekker, Nat. Mater. **2**, 537 (2003).
[26] V. Tabard-Cossa, D. Trivedi, M. Wiggin, N. N. Jetha, and A. Marziali, Nanotechnology **18**, 305505 (2007).
[27] R. M. M. Smeets, N. H. Dekker, and C. Dekker, Nanotechnology **20**, 095501 (2009).
[28] S. W. Kowalczyk, D. B. Wells, A. Aksimentiev, and C. Dekker, Nano Lett. **12**, 1038 (2012).
[29] Y. H. Sen and R. Karnik, Anal. Bioanal. Chem. **394**, 437 (2009).
[30] A. J. Storm, J. H. Chen, H. W. Zandbergen, and C. Dekker, Phys. Rev. E **71**, 051903 (2005).
[31] S. Liu *et al.*, Adv. Mater. **25**, 4549 (2013).
[32] S. Garaj, S. Liu, J. A. Golovchenko, and D. Branton, Proc. Natl. Acad. Sci. USA **110**, 12192 (2013).
[33] M. Wanunu, J. Sutin, B. McNally, A. Chow, and A. Meller, Biophys. J. **95**, 4716 (2008).
[34] G. M. Skinner, M. van den Hout, O. Broekmans, C. Dekker, and N. H. Dekker, Nano Lett. **9**, 2953 (2009).
[35] D. Fologea, J. Uplinger, B. Thomas, D. S. McNabb, and J. L. Li, Nano Lett. **5**, 1734 (2005).
[36] B. Q. Luan, G. Stolovitzky, and G. Martyna, Nanoscale **4**, 1068 (2012).
[37] A. Meller and D. Branton, Electrophoresis **23**, 2583 (2002).
[38] M. Wanunu, W. Morrison, Y. Rabin, A. Y. Grosberg, and A. Meller, Nat. Nanotechnol. **5**, 160 (2010).

[39] N. An, A. M. Fleming, and C. J. Burrows, J. Am. Chem. Soc. **135**, 8562 (2013).

[40] N. An, A. M. Fleming, E. G. Middleton, and C. J. Burrows, Proc. Natl. Acad. Sci. USA **111**, 14325 (2014).

[41] D. Koirala, S. Dhakal, B. Ashbridge, Y. Sannohe, R. Rodriguez, H. Sugiyama, S. Balasubramanian, and H. B. Mao, Nat. Chem. **3**, 782 (2011).

[42] J. Shim and L. Q. Gu, Methods **57**, 40 (2012).

[43] M. Zwolak and M. Di Ventra, Rev. Mod. Phys. **80**, 141 (2008).